A 1.54mm² Wake-Up Receiver Based on THz Carrier Wave and Integrated Cryptographic Authentication

Eunseok Lee[1], Muhammad Ibrahim Wasiq Khan[1], Xibi Chen[1], Utsav Banerjee[2], Nathan Monroe[1], Rabia Tugce Yazicigil[3], Ruonan Han[1], Anantha P. Chandrakasan[1]

[1]Massachusetts Institute of Technology, USA,
[2]Indian Institute of Science, India, [3]Boston University, USA

2023 IEEE Custom Integrated Circuits Conference (CICC) | 979-8-3503-9948-6/23/$31.00 ©2023 IEEE | DOI: 10.1109/CICC57935.2023.10121285

Distributed, mass-deployable mm-sized nodes with communication, sensing, and actuation capabilities such as microbots [1] and THz radios [2] are the key components of future collaborative large-scale networks with minimum intrusion. This vision is enabled by devices with miniaturization, low-cost fabrication, and low power. There is, therefore, a growing interest in mm-sized wake-up receivers (WuRxs) to save the limited battery energy of those devices. The size of RF WuRx is determined by the antenna, which is fundamentally proportional to the square of the carrier wavelength and is typically at cm² level in the GHz range [3]. Using higher carrier frequency of 78GHz, the work in [4] demonstrates the previously smallest RF-WuRx size of 49mm², but at the expense of high DC power of 25mW. Other modalities are also adopted for size reduction. In [5], an ultrasonic (US) WuRx is presented with a size of 14.5mm², but requires an off-chip US transducer. In [6], an optical WuRx reduces the size to 0.85mm² through integrated photodiodes, but the operation is susceptible to ambient light interference.

This paper demonstrates the first THz WuRx that uses a 264GHz carrier wave to enable on-chip antenna integration and >10x size reduction compared to [4]. The receiver has a size of only 1.54mm², -48dBm sensitivity and 2.88μW DC power at a 1.02kbps data rate. The utilization of highly directive and potentially steerable THz beam also provides improved security and spatial selectivity. The architecture of the WuRx is shown in Fig. 1, of which the THz frontend is based on a pair of dual-antenna-feed, pseudo-differential CMOS THz detectors, and an amplifier-filter-comparator chain. While prior WuRx chips use predefined tokens that can be eavesdropped and reused in Denial-of-Sleep attacks (a critical threat for mm-sized platforms due to the small battery size), this work implements a built-in low-power authentication block that randomizes tokens using a lightweight cryptographic algorithm.

The THz receiver front end shown in Fig. 2 is pseudo-differential and consists of a NMOS and PMOS detector with opposite responsivity polarities. The MOSFETs have zero static channel current to eliminate power consumption and flicker noise. Meanwhile, a dual-antenna topology, which is previously applied for energy harvesting [7], is adopted for low noise equivalent power (NEP) and high responsivity; the former sets the upper limit of the WuRx sensitivity and the latter relaxes the gain and noise requirements of the amplifier stages, thus reducing DC power. In a conventional MOSFET THz detector topology (Fig. 2), the drain and gate are coupled through an explicit or parasitic capacitor (C_e). Hence, the voltages of the two nodes are almost identical ($v_{ds} \approx v_{gs}$). However, the peak responsivity of 26.8kV/W occurs near $\angle(v_{ds}/v_{gs})=170°$ and $|v_{ds}/v_{gs}|= 4.5$, which is 2x higher than that at $v_{ds}/v_{gs}=1$. These two optimal conditions along with antenna-to-device matching are difficult to achieve simultaneously in a single-antenna, low-complexity (hence low-loss) topology. This is addressed in the dual-antenna topology (Fig. 2) by de-coupling the designs of ratioed power feeding and impedance matching between the gate and drain. The two patch antennas placed back-to-back directly provide near-180° phase difference between v_{ds} and v_{gs}. Next, changing the widths of the patches (W_D and W_G) hence the corresponding antenna gains (Fig. 2) allows for independent adjustment of the ratio between THz power (P_D/P_G) injected into the drain and gate. With W_G=200μm and W_D= 600μm, the resultant P_D/P_G is 2.54, and $|v_{ds}/v_{gs}|$ reaches the desired value of 4.5. The Smith chart for the matching network of the NMOS detector is shown in Fig. 2. The simulated NMOS detector has a responsivity of 13.3kV/W including matching networks losses, 4.4kV/W with 34% antenna efficiency, and an overall NEP of 8.2pW/Hz$^{1/2}$. Similarly, the PMOS detector achieves a simulated responsivity of 3.4kV/W and NEP of 8.6pW/Hz$^{1/2}$. The central AC grounds of the patch antennas are used for DC gate biasing and extracting the demodulated signals from drain nodes with no disturbance to THz operation.

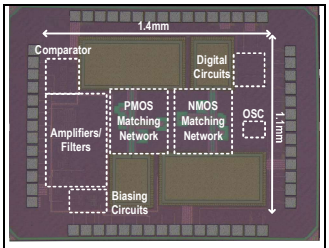

Die micrograph.

The THz frontend connects directly to the baseband chain (Fig. 3), which consists of an LNA, HPFs, VGAs, and a gm-C filter. The output noise spectrum of the baseband chain, the THz frontend, and their sum are shown in Fig. 3, with the passband band gain of 51dB and DC power of 2.64μW. Finally, the output is connected to a comparator with -30 to 30mV controllable offset. The WuRx can also bit-level duty cycle (BLDC) the amplifier-filter chain, which consumes 96% of the total power.

The authentication block diagram is shown in Fig. 3. The token consists of a preamble, a counter, and an encrypted counter. With successful authentication, the WuRx issues the wake-up and updates the token using the key and counter. If the counter desynchronizes between Tx and WuRx, packet control logic resynchronizes the counter using the received token. The counter is encrypted by GIFT, a lightweight cipher for resource-constrained devices. We implement GIFT-64, which has a block size of 64 bits and a key size of 128 bits. The entire digital circuit occupies 11.6kGE and is synthesized using HVT devices to reduce leakage power. It consumes 33.6nW static and 65nW total measured power under the ~10kHz clock and 0.8V power supply. Notably, this security feature has been added to the system while adding a few tens of nWs of power. The clock is generated by a 4b-tunable leakage-based oscillator consuming a maximum measured power of 18.5nW.

The chip is fabricated in 65nm CMOS process and has an area of 1.54mm². Unlike [3-5], no external antenna or transducer is needed. The test setup in Fig. 4 is used to measure the performance of the THz detector and WuRx. The responsivity is measured at a far-field distance of 25cm using a lock-in amplifier and a VDI-WR3.4-VNAX, which radiates a -6.2dBm 264.3GHz signal through a 25dBi horn antenna. The noise spectral density of the THz detector is 60dB amplified by an ultra-low noise preamplifier and measured using a vector signal analyzer. The measured minimum NMOS detector NEP is 10.5pW/Hz$^{1/2}$ at V_{GS}=0.35V. The measured frequency selectivity and angle sensitivity are presented in Fig. 4. The E-plane is more sensitive to the H-plane because the non-zero azimuth angle provides an extra phase difference between two antenna outputs, disrupting the optimal condition. Note that angle sensitivity is not the radiation pattern. In addition, a sensitivity of -48dBm with 10^{-3} BER is achieved under the 2.88μW measured power and 1.02kbps data rate, as shown in Fig. 5. With a 20% BLDC of the amplifier-filter chain, a sensitivity of -47.8dBm and data rate of 86.6bps are obtained while reducing the average power to 748nW. Fig. 5 also shows the authenticated wake-up protocol scenarios and its time-domain waveform. The wake-up was only issued when valid tokens were successfully received.

Next, a wireless setup based on a VDI amplifier-multiplier chain (P_{out} =90mW) is utilized to demonstrate longer-range communication (Fig. 5). At extended distances of 5.1m and 7.6m, the measured BERs are 5.7×10^{-3} and 1.7×10^{-3}, respectively. To relieve the requirement of fixed interrogator-WuRx alignment, a demo using a beam-steering THz reflectarray [8] at the interrogator side is carried out. Upon the focusing from the reflectarray, the 1°-wide 264.3GHz beam is guided towards different directions and is OOK modulated at 487.5Hz. The FFT results show that the signal is detected in different locations. The SNR limited by the reflectarray losses precludes complete recovery of the OOK signal, but the demo illustrates how distributed nodes is addressed through a central THz hub in the future. Fig. 6 shows the wavelength versus the power-sensitivity product among WuRxs using the RF-to-THz spectrum, where the presented work demonstrates the smallest size and pushes the boundary of the design trade space with a low-cost, fully-integrated solution. A comparison with mm²/cm²-sized WuRxs is shown in Fig. 6.

References:

[1] R. Casanova, *et al.*, *ISSCC* 2009 [2] E. F. Garay, *et al.*, *JSSC* 2022
[3] K. Sadagopan, *et al., RFIC* 2017 [4] M. Dadash, *et al.*, *IMS* 2017
[5] A. S. Rekhi, *et al.*, *ISSCC* 2018 [6] W. Lim, *et al.*, *VLSI* 2016
[7] M. I. W. Khan, *et al.*, *RFIC* 2022 [8] N. Monroe, *et al.*, *ISSCC* 2022

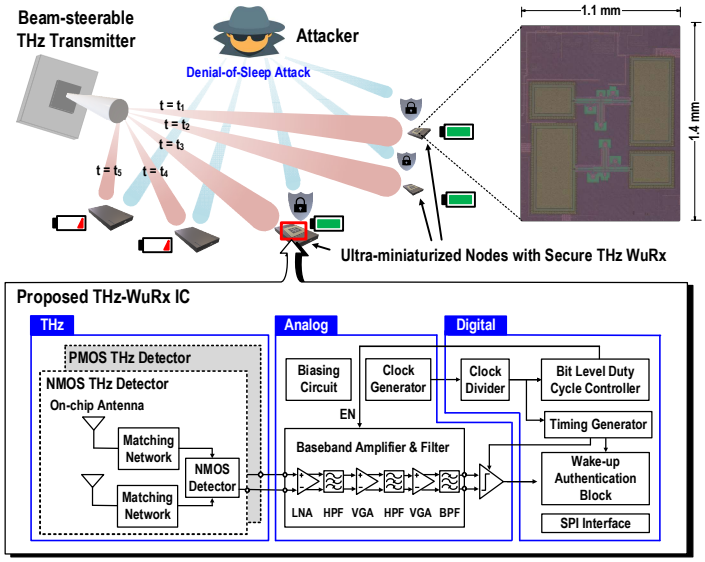

Fig. 1. Application scenario of using secure THz WuRx with ultra-miniaturized nodes and the block diagram of the proposed WuRx

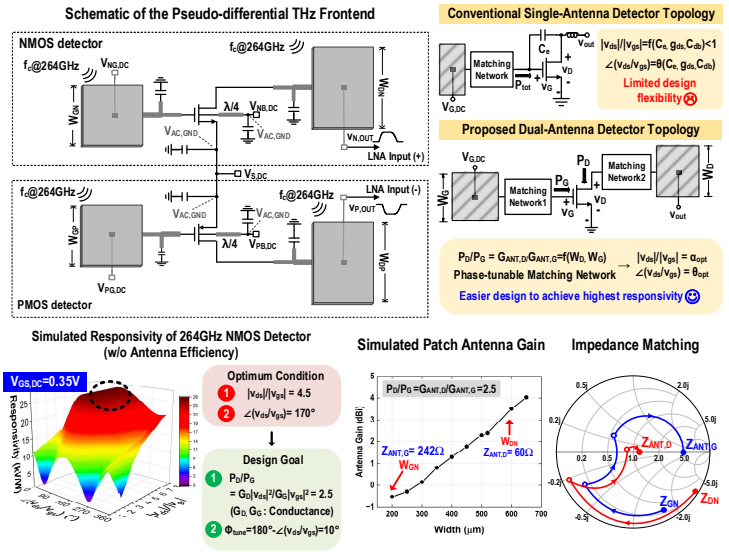

Fig. 2. Schematic of the THz frontend, simulated detector and antenna performances and Smith chart for optimum condition

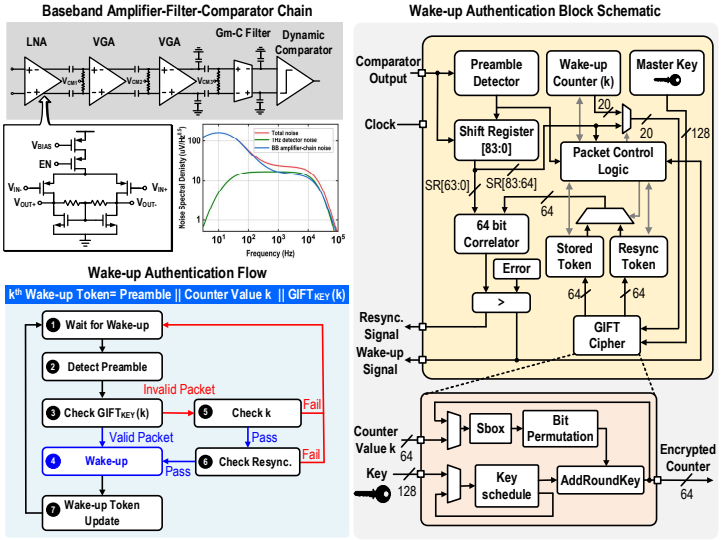

Fig. 3. Schematic of the baseband chain and noise spectral density, proposed wake-up authentication flow and block schematic

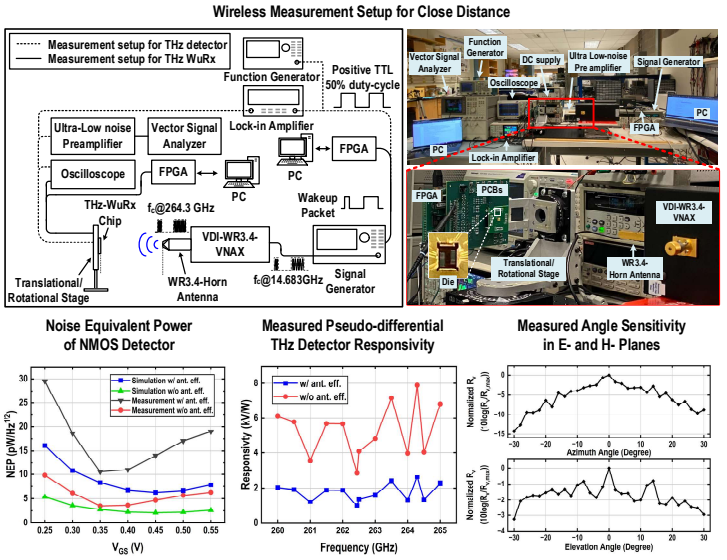

Fig. 4. Wireless measurement setup for THz detector and WuRx at close distance, measured performances of THz detector

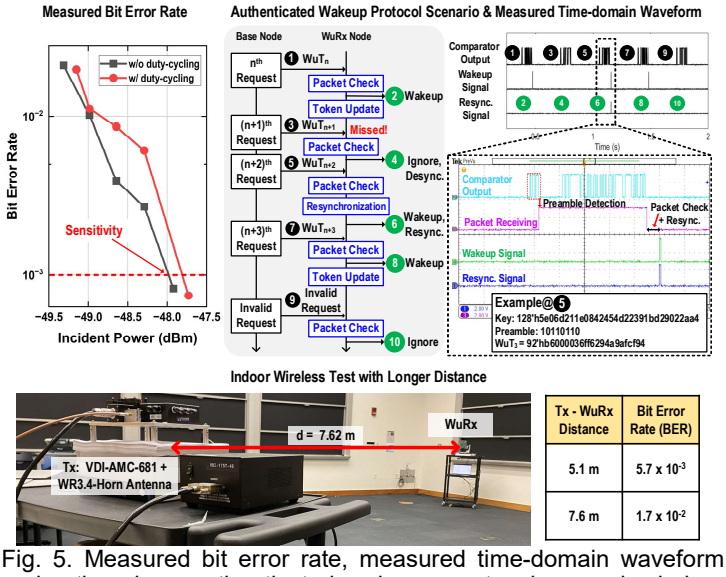

Tx - WuRx Distance	Bit Error Rate (BER)
5.1 m	5.7 x 10^{-3}
7.6 m	1.7 x 10^{-2}

Fig. 5. Measured bit error rate, measured time-domain waveform under the given authenticated wake-up protocol scenario, indoor wireless test with longer-range

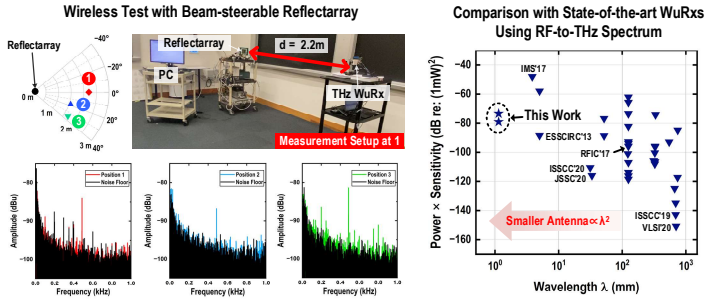

Comparison with the State-of-the-art Radiator-integrated mm²/cm²-sized WuRxs

Metric	Lim, VLSI'16	Dadash, IMS'17	Sadagopan, RFIC'17	Rekhi, ISSCC'18	Jiang, JSSC'20	This Work
Transmit Medium	Optical	mmWave	RF	Acoustic	RF	THz
Carrier Frequency	352.9THz	78GHz	2.4GHz	~ 57kHz	9GHz	264GHz
Die Active Area	0.85mm²	0.44mm²	1.1mm²	1.5mm²	4/12mm²	1.54mm²
System Area / Aperture	0.85mm²	49mm²	187.5mm²	14.5mm²	450mm²	1.54mm²
Process Node	180nm CMOS	55nm SiGe BiCMOS	65nm CMOS	65nm CMOS	65 / 180nm CMOS	65nm CMOS
Data Rate	5bps	Not Shown	2.5kb/s	336bps	33.3bps	1.02kbps / 86.6bps [a]
Sensitivity	-30.5dBm	-62dBm	-61.5dBm	-59.7dBm	-69.5dBm	-48dBm / -47.8dBm [a]
Power	380pW	25mW	365nW	8nW	22.3nW	2.88μW / 750nW [a]
External off-chip components	No	Antenna	Antenna	Transducer	Antenna	No
Beam-steering test?	No	No	No	No	No	Yes
Security	No	No	No	No	No	Yes

[a]20% bit-level duty-cycling

Fig. 6. Demonstration of wireless communication pairing with beam-steerable reflectarray, comparison with the state-of-the-art WuRxs